Low lattice thermal conductivity in alkali metal based Heusler alloys

Utkarsh Singh,[1,*] Sapna Singh,[1,*,†] Mohd Zeeshan,[1] Jeroen van den Brink,[2,3] and Hem C. Kandpal[1,‡]

[1]*Department of Chemistry, Indian Institute of Technology Roorkee, Roorkee 247667, Uttarakhand, India*

[2]*Institute for Theoretical Solid State Physics, IFW Dresden, Helmholtzstrasse 20, 01069 Dresden, Germany*

[3]*Institute for Theoretical Physics and Würzburg-Dresden Cluster of Excellence ct.qmat, Technische Universität Dresden, 01069 Dresden, Germany*

(Received 16 June 2022; accepted 22 November 2022; published 12 December 2022)

On the basis of purely their electronic properties, semiconducting alkali and alkaline earth metal based Heusler alloys have been identified as potentially promising thermoelectrics. Their thermal transport properties are decisive and help to further gauge this potential. This motivates us to systematically investigate lattice properties of three eight valence electron Heusler alloys, namely, Li_2NaSb, Na_2KSb, and K_2CsSb, using first-principles approaches. On the basis of both qualitative and quantitative descriptors (assessing covalent bonding, the atomic displacement parameter, the phonon density of states, the Grüneisen parameter, the phonon group velocity, and the phonon lifetime) we analyze in detail the lattice degrees of freedom and their contribution to thermal transport. Out of the three materials, Na_2KSb and K_2CsSb exhibit surprisingly low lattice thermal conductivity, which we can attribute to the anharmonic rattling of the loosely bound alkali atom in the crystal lattice. K_2CsSb has a lattice thermal conductivity two times lower than that of SnSe, a material with a record figure of merit.

DOI: 10.1103/PhysRevMaterials.6.125401

I. INTRODUCTION

Favorable thermal transport properties that retain a good power factor could be a boon for developing next-generation thermoelectric (TE) materials. Recently, He *et al.* [1] predicted ultralow lattice thermal conductivity in alkaline earth metal based full Heusler (FH) alloys X_2YZ (X = Ca, Sr, and Ba; Y = Au and Hg; Z = Sn, Pb, As, Sb, and Bi) owing to strong anharmonic rattling of the heavy noble metals. Such ultralow lattice thermal conductivity in the cubic crystal structure of FH is unprecedented and contrary to the belief that complex, large unit cells are required for low thermal conductivity. In addition, alkali and alkaline metal based FH alloys have been sporadically considered as TE materials. An example of a relatively widely studied FH is Fe_2VAl [2–7], which shows impressive electrical transport achieved via doping. However, its thermoelectric performance is rather limited due to intrinsically high lattice thermal conductivity. Even though the FH class of alloys has not been very impressive as thermoelectrics, based on an analysis of purely electronic degrees of freedom, Xing *et al.* [8] were able to identify alkali metal based FH Li_2NaSb and K_2CsSb as alloys with electronic properties superior to those of Fe_2VAl at low and moderate doping levels. This motivates a detailed analysis of lattice degrees of freedom and their contribution to thermal transport for such systems.

The crystal structure of FH X_2YZ allows the Y atoms to rattle in a relatively strongly bonded X-Z sublattice. There could be more or less rattling depending on the bonding of Y atoms with the lattice. A strong anharmonic rattling of atoms may significantly reduce the lattice thermal conductivity. Further, the 18-Valence electron count FH alloys have a closed shell electronic structure and are mostly semiconducting, in accordance with the Slater-Pauling rule. This warrants good electrical transport properties.

To the best of our knowledge, experimentally, Na_2KSb and K_2CsSb have been studied in detail with respect to their optical properties as photocathode materials [9–11], with some results published as recently as 2017. Although the crystal structure of Li_2NaSb has been studied, it has not been of much interest for applications as a photocathode [12]. All three alloys have been shown to crystallize in fcc symmetry and are insulators.

In this work, using first-principles calculations, we demonstrate that low thermal conductivity accompanies the favorable electronic transport characteristics in FH Li_2NaSb, Na_2KSb, and K_2CsSb. Particularly in Na_2KSb and K_2CsSb, the room temperature lattice thermal conductivity is found to be so low that it approaches the theoretical minimum. To analyze and account for such low thermal conductivity, we investigate the bonding, lattice dynamics, and phonon transport in the system. The electrical transport properties are also computed to obtain a comprehensive measure of thermoelectric performance, i.e., the figure of merit.

This paper is organized as follows: Sec. II briefly describes the computational techniques utilized for calculating the electronic structure and electrical and thermal transport properties. Section III presents the results for phonon dispersions, lattice thermal conductivity, and electrical transport coefficients. A summary of the paper is presented in Sec. IV.

*These authors contributed equally to this work.

†Present address: Linköping University, Department of Physics, Chemistry and Biology (IFM), SE-581 83 Linköping, Sweden.

‡Corresponding author: hem.kandpal[at]cy.iitr.ac.in

TABLE I. Calculated room temperature lattice thermal conductivity, average sound velocity, bulk modulus, Grüneisen parameter, and minimum theoretical thermal conductivity of Li_2NaSb, Na_2KSb, and K_2CsSb along with experimentally reported data for some relevant systems.

System	κ_L (W m^{-1} K^{-1})	υ_s (km s^{-1})	B (GPa)	γ	κ_{glass} [a], κ_{diff} [b] (W m^{-1} K^{-1})
Li_2NaSb	4.50	4.98	29	3.8	0.71, 0.59
Na_2KSb	0.75	4.30	20	3.3	0.47,0.38
K_2CsSb	0.20	2.95	12	2.7	0.26, 0.21
Fe_2VAl [3]	28.0				
FeTaSb [31]	8.80	2.9			
BiCuSeO [35]	0.55	2.1		1.5	
SnSe [32]	0.47	2.0		7.2	

[a] $\kappa_{L,min}$ from Clarke's model [34].
[b] $\kappa_{L,min}$ from the diffusive transport model [34].

II. COMPUTATIONAL METHODS

The electronic structure calculations at the level of density functional theory were performed with the Vienna Ab initio Simulation Package (VASP) [13–16] within the generalized gradient approximation (GGA) as parametrized by Perdew, Burke, and Ernzerhof [17,18]. The all-electron projector augmented wave [19,20] method was adopted with a plane-wave cutoff energy of 760 eV due to the presence of lithium in one of the systems. Both atomic positions and lattice parameters were allowed to relax using a Γ-centered k-point sampling of $41 \times 41 \times 41$ until the convergence criterion of 10^{-8} for total energy and 10^{-7} for Hellmann-Feynman forces was achieved.

Both second- and third-order interatomic force constants (IFCs) were calculated via the finite displacement method using a $2 \times 2 \times 2$ conventional supercell (128 atoms). The second-order IFCs in the harmonic approximation were calculated using the PHONOPY [21] package, and third-order (anharmonic) IFCs as well as thermal conductivity were calculated using the PHONO3PY [22] package. For the lattice thermal conductivity calculation, the direct solution [23] method of the linearized Boltzmann transport equation for phonons as implemented in PHONO3PY was used with a $15 \times 15 \times 15$ q mesh. We tested the convergence of lattice thermal conductivity with the q grid by gradually increasing the density of q points, and a $15 \times 15 \times 15$ q grid was found to provide precise values up to 10^{-3} W m^{-1} K^{-1}. The crude force-constant approximation with a decreased cutoff distance for three-phonon processes was not used.

The electrical transport properties were calculated with a dense k mesh of $47 \times 47 \times 47$ by iteratively solving the linearized Boltzmann transport equation for electrons as implemented in the BOLTZTRAP2 code [24]. EPW [25] coupled with QUANTUM ESPRESSO [26,27] was utilized to calculate electronic relaxation times. To calculate e-ph coupling matrix elements, Γ-centered $12 \times 12 \times 12$ and $8 \times 8 \times 8$ grids were utilized to sample the electron and phonon momentum spaces, respectively, with a plane-wave energy cutoff of 90 Ry. Wannier interpolation was performed using the PW2WANNIER90.X module. To calculate the electron self-energy, a broadening of 15 meV was found to be sufficient, with 10^6 random k and q points for numerical integration. STUTTGART TB-LMTO-ASA [28] was used to investigate the bonding and calculate crystal orbital Hamilton population (COHP) and integrated crystal orbital Hamilton population (ICOHP) values.

III. RESULTS AND DISCUSSION

A. Lattice dynamics

The calculated lattice thermal conductivity κ_L for all three alloys at room temperature is presented in Table I. The temperature-dependent values are illustrated in Fig. 1. It is important to note that Na_2KSb [29,30] and K_2CsSb [11,30] are prone to structural instability beyond room temperature, while Li_2NaSb [12] can be stable up to 1100 K. Hence, their properties are explored only near 300 K, which is the temperature of interest in this work. The values obtained are significantly lower in comparison to typical Heusler and half-Heusler alloys like Fe_2VAl [3] and FeTaSb [31], respectively, which have been studied in detail owing to their promising thermoelectric properties. Interestingly, we also find that κ_L of K_2CsSb is two times lower than that of SnSe [32], a material with a record figure of merit. It should also be noted that this value approaches the amorphous limit [33,34]. In fact, the calculated κ_L for K_2CsSb is even slightly lower than the theoretical minimum, which is attributed to the uncertainties in the

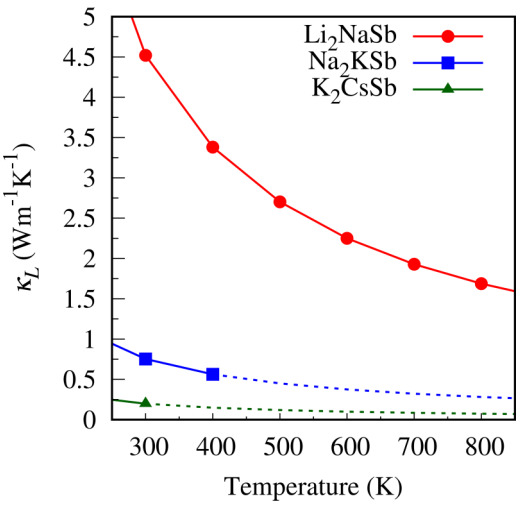

FIG. 1. Lattice thermal conductivity as a function of temperature for Li_2NaSb, Na_2KSb, and K_2CsSb.

TABLE II. Integrated crystal orbital Hamiltonian populations (COHPs) for pairwise interactions in Li_2NaSb, Na_2KSb, and K_2CsSb.

	Integrated COHP (eV per interaction)			
	Li_2NaSb	Na_2KSb	K_2CsSb	Fe_2VAl
X-*Y*	0.05	0.05	0.02	2.21
X-*Z*	0.40	0.35	0.22	1.43
Y-*Z*	0.25	0.02	0.07	0.10

calculated phonon band structures and the anharmonic force constants. A summary of the minimum thermal conductivity defined by different minimum thermal conductivity models [34] is presented in Table I.

We observe in systems like SnSe [32] and BiCuSeO [35] that crystal structure and bonding play an important role in the reduction of lattice thermal conductivity. These alkali metal based Heusler alloys are unlike their conventional counterparts (X_2YZ), where *X* and *Y* are both transition metal elements and *Z* is a main group element. Naturally, we expect the bonding characteristics to be different as well. While it is expected that in transition metal based Heusler alloys, covalent and metallic bonding will be the dominant interactions, we posit that in our systems, covalent interaction will be significantly weaker due to the ionic nature of alkali metals. To ascertain the extent of covalent bonding, we perform COHP analysis for each system and also calculate the ICOHP up to the Fermi level ϵ_F for each pairwise interaction, which quantifies covalent bonding in the system (Table II). While the trends in the *X*-*Z* interaction and *Y*-*Z* interactions remain the same, the interaction strength between the *X*-*Y* pair is significantly lower in all three systems, indicating that the *Y* atom is loosely bonded to the lattice, in stark contrast to, for instance, Fe_2VAl.

This points us to a Zintl-like picture [36], where the *Y* atom engages in ionic bonding within the *X*-*Z* framework. Of course, the interaction strength of the *X*-*Z* framework also decreases as we go down the group to K_2CsSb (Table II), owing to the increased ionic character of the *X* atom. On account of a single atom, evidently loosely bonded to the lattice, we naturally suspect this atom is highly prone to thermal fluctuations compared to other atoms in the lattice. To investigate this, we calculated the atomic displacement parameter (ADP) for all the atoms in the system with varying temperatures.

Figure 2 illustrates the ADPs of different atoms in all three systems for varying temperatures. Unsurprisingly, ADPs of *Y* atoms in the respective alloys turn out to be larger than those of other constituents, further confirming the nature of bonding in the lattice. It has been shown that a room temperature ADP can be used to identify alloys with unusually low κ_L [37]. For Li_2NaSb and Na_2KSb, the room temperature ADPs of Na and K, respectively, are appreciable and comparable to those of systems containing guest rattler atoms. However, the difference between thermal motions among all atoms in their respective systems is not significant. The case of K_2CsSb is particularly interesting as the ADP value of Cs (0.06 $Å^2$ at 300 K) is of the same order as that of Tl (0.07 $Å^2$ at 300 K) in $TlInTe_2$ [38], a system which boasts an ultralow value of κ_L owing to intrinsic rattling. Our calculated ADPs, coupled with the nature of bonding in these alloys, which is quantified by ICOHP values, suggest that the loosely bonded atom indeed acts as an intrinsic rattler, thus scattering heat-carrying phonons and lowering κ_L.

Part of exploring the lattice dynamics is also to examine the nature of vibrations in the lattice, which can be harmonic or anharmonic. The presence of anharmonic vibrations in the lattice, also known as lattice anharmonicity, is well known to reduce κ_L in crystalline structures [32,39]. To qualitatively measure the extent of anharmonicity in the system, we calculate the mode Grüneisen parameters γ, defined as $\gamma_{qv} = -\frac{dln\omega_{qv}}{dlnV}$, using a central difference formula taking phonon frequencies calculated at ±2% of the equilibrium volume for each alloy (Table I).

A larger γ indicates larger anharmonicity in the lattice. In fact, such irregular (anharmonic) motion of certain atoms in the system, also known as rattlers, is associated with increased phonon scattering, an important mechanism for reducing lattice thermal conductivity. Hence, a larger ADP, which is defined as the vibrational motion around the equilibrium position, also implies large anharmonicity in the alloy. The

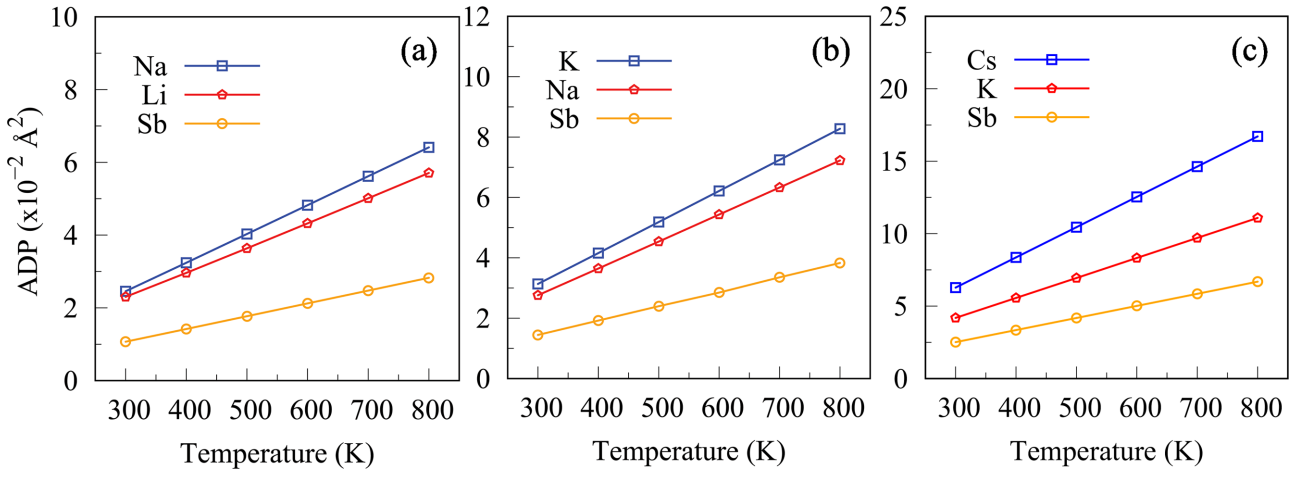

FIG. 2. Atomic displacement parameters for (a) Li_2NaSb, (b) Na_2KSb, and (c) K_2CsSb.

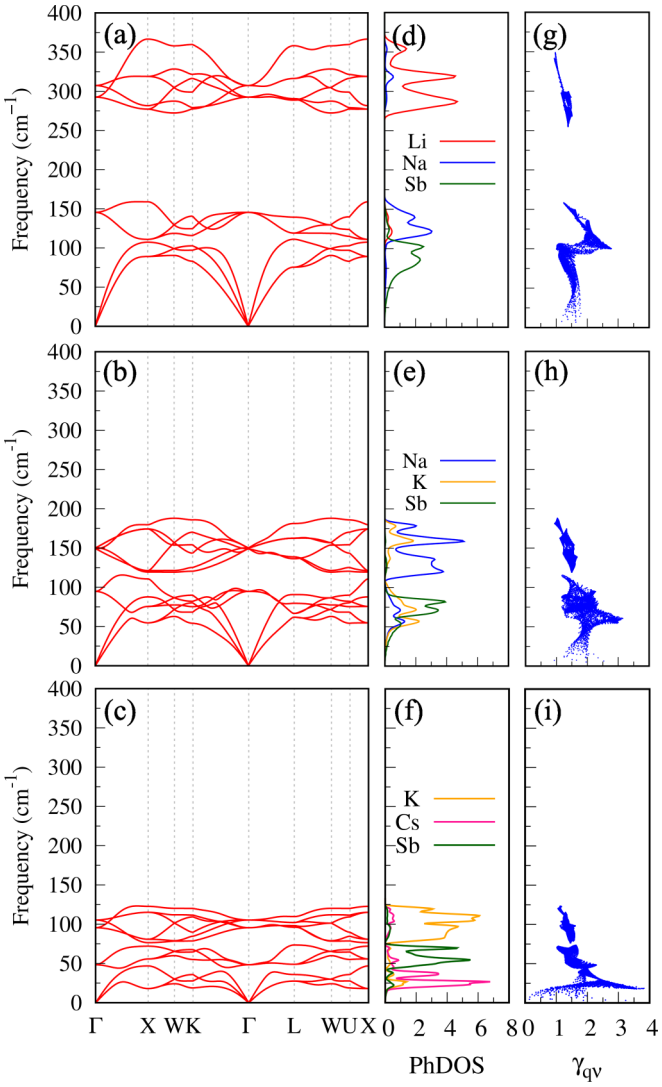

FIG. 3. (a)–(c) Phonon dispersions, (d)–(f) partial phonon density of states, and (g)–(i) Grüneisen parameter of Li_2NaSb, Na_2KSb, and K_2CsSb, respectively.

benchmark we looked at is SnSe, in which anomalously large anharmonic vibrations ($\gamma \sim 7.2$) owing to soft bonding [32] lead to a very low κ_L. We obtained a high value of $\gamma \sim 3.8$ in K_2CsSb which decreases gradually to 2.75 in Li_2NaSb in the acoustic region (Fig. 3). The γ values indicate strong anharmonicity in K_2CsSb compared to Na_2KSb and are lowest in Li_2NaSb, a trend which is reflected in κ_L as well (Fig. 1).

B. Thermal transport

By examining the nature of bonding and vibrations, we have clarified the role of rattlers in suppressing κ_L. However, the way these vibrations, quantified as phonons, propagate throughout the lattice still needs to be understood. Determining how heat carriers at different energies (frequencies) behave in the Brillouin zone (BZ) and contribute to thermal transport is hence relevant. To do so, we calculate how phonon modes at different frequencies propagate through the lattice and how different atoms in the lattice contribute to thermal transport.

Figure 3 shows the phonon dispersions and phonon density of states (PhDOS, states cm^{-1}) in Li_2NaSb, Na_2KSb, and K_2CsSb. In all three systems, the high-frequency optical modes are dominated by phonons originating from the lighter element, which is expected. The band gap between low-lying optical (LLO) modes and high-lying optical (HLO) modes is naturally the largest in Li_2NaSb owing to Li being much lighter than other constituents of these systems. In fact, the vibrations in the lattice are capped at much lower frequencies for K_2CsSb ($\sim$180 cm^{-1}) compared to Li_2NaSb ($\sim$400 cm^{-1}), which is expected since the average molecular mass increases significantly as we go down the group to K_2CsSb. Suppressed phonon mode frequencies lead to flat, dispersionless bands in Na_2KSb, which is even more pronounced in K_2CsSb. K_2CsSb, in particular, exhibits very interesting features in its band structure as a large avoided crossing is observed between the acoustic and LLO branches, which bolsters the evidence for the presence of rattling modes in the system [40].

Since we already know that Cs shows significant rattling, it will be interesting to see its contribution to the phonon modes as well as thermal conductivity. PhDOS of K_2CsSb exhibits highly localized phonon modes of each atom. While phonon modes from Cs atoms entirely dominate the acoustic region, the majority of LLO modes are contributed by Sb atoms, and as expected, K atoms contribute the HLO modes. Similar features are observed in Li_2NaSb as well, where a very small avoided crossing at the X point is observed. We also see localization in Li_2NaSb, where Sb atoms account for most acoustic modes and Na atoms contribute mostly to LLO modes. Since we now understand how individual atoms contribute phonon modes to the system, we can look at how thermal transport is governed. To quantify the contribution of phonon modes at different frequency ranges, we calculate the variation of cumulative lattice thermal conductivity with frequency (Fig. 4).

While both acoustic and LLO modes originating from Na and Sb atoms contribute to lattice thermal conductivity in Li_2NaSb (95%), the contribution of acoustic modes with respect to LLO modes increases significantly as we go down to K_2CsSb. In fact, for Na_2KSb, acoustic modes contribute $\sim$53% of κ_L, while LLO modes contribute $\sim$27%. This separation increases even more in K_2CsSb, where acoustic modes contribute $\sim$63% of κ_L and LLO modes contribute $\sim$13%. Another common feature we observe as we go to K_2CsSb is the increased contribution of HLO modes to κ_L.

While the decrease in the LLO-HLO band gap provides for higher participation of HLO modes in phonon transport, the scattering channels at higher frequencies also become available, hence contributing to the reduction of κ_L. With this, we get a qualitative understanding of thermal transport through this analysis, and it would be beneficial to obtain a quantitative understanding as well. We now inspect the parameters that have a direct relation to κ_L.

Classically, lattice thermal conductivity is expressed as $\kappa_L = \frac{1}{3} C_V v^2 \tau$, where C_V is the heat capacity at constant volume; v is the sound velocity, also understood as the velocity of phonons at the zone center; and τ is the phonon

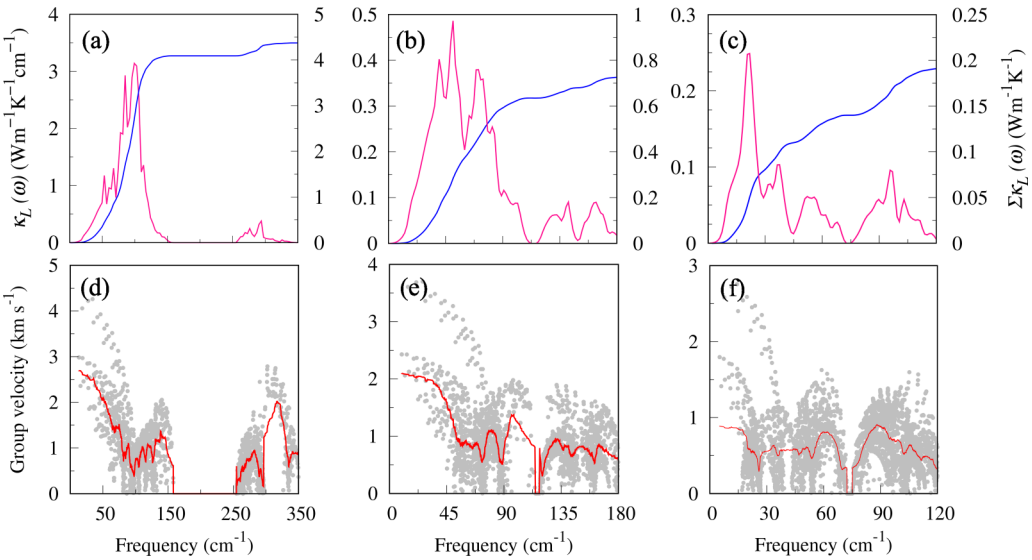

FIG. 4. (a)–(c) Slope of the lattice thermal conductivity and cumulative lattice thermal conductivity and (d)–(f) group velocities as a function of phonon frequencies of Li_2NaSb, Na_2KSb, and K_2CsSb, respectively.

lifetime. Hence, κ_L can be understood to be influenced by two important parameters which quantify the movement of heat carriers: phonon velocity and phonon lifetime. We calculate the phonon group velocity $v_g = \frac{\partial k}{\partial \omega}$ (Fig. 4) as well as the speed of sound v_s, which is approximated by the formula $\frac{3}{v_s^3} = \frac{1}{v_{LA}^3} + \frac{1}{v_{TA_I}^3} + \frac{1}{v_{TA_{II}}^3}$ near the zone center (Γ point) where ω varies linearly with k for all three systems (Table I). The mean group velocities, indicated by the moving average line in Fig. 4 as well as v_s, decrease from Li_2NaSb to K_2CsSb. The trends in mean sound velocity v_s can be explained by a simplified relation with bonding in the system and the average atomic mass expressed as $v_s \sim \sqrt{k/M}$, where k is the force constant and M is the average atomic mass. Clearly, alloys with softer bonding in the system, indicated by their bulk modulus (Table I) and ICOHP values, as well as heavier atoms will have lower sound velocities and, following the above-stated relation, lower κ_L. As explored earlier, while the majority of heat carriers in Li_2NaSb are acoustic phonons, in Na_2KSb and K_2CsSb, higher-frequency optical modes also contribute significantly, and hence, the movement of optical phonons also becomes important in these cases. We see that the phonon group velocities in acoustic and optical regions follow the same trends as κ_L in both these alloys, indicating that the majority of heat carriers are slow. Interestingly, the sound velocity in K_2CsSb is comparable to those of some of the reported alloys with low κ_L, such as BiCuSeO (2.1 km s^{-1}) and SnSe (2.0 km s^{-1}).

In addition to the group velocities, which indicate the speed of heat carriers in the system, the trends in κ_L also originate from the scattering rates of phonons, indicated by phonon lifetimes in the Brillouin zone. We find that for Li_2NaSb, the heat-carrying phonons (~140 cm^{-1}) have a lifetime close to 2 ps. For Na_2KSb and K_2CsSb, even lower lifetimes of 0.7 ps (~80 cm^{-1}) and 0.35 ps (~50 cm^{-1}), respectively, are found. The appreciable differences in τ for each alloy reflect the trend in κ_L values excellently, indicating that in addition to the heat carriers being slow, phonon scattering processes resulting in smaller lifetimes provide an important mechanism for reduction of κ_L. The lifetime plots are given in the Supplemental Material [41].

Thus, by examining qualitative descriptors, the ADP, ICOHP, and Grüneisen parameters supplemented with the inference obtained from phonon dispersions and PhDOS, as well as quantitative descriptors in (v_g, v_s) and τ, we established the origin of the low thermal conductivity and the nuances of thermal transport in our systems. Motivated by the presence of favorable thermal transport and previous studies performed by Xing *et al.* [8], which proposed these systems are good thermoelectrics, albeit based on electronic properties alone, we now go on to explore and model in considerable detail the electrical transport properties of these alloys to gauge their potential as practical thermoelectrics and estimate their figure of merit.

C. Electrical transport properties

The thermoelectric performance of a material is given by the figure of merit, $ZT = S^2\sigma T/(\kappa_e + \kappa_L)$, where S is the Seebeck coefficient, σ is the electrical conductivity, and κ_e and κ_l are the electronic and lattice contributions to the thermal conductivity, respectively. The electrical transport coefficients (S, σ, κ_e) are calculated within the constant relaxation time approximation and rigid band approximation, which have been successfully utilized to find new thermoelectric materials. As semilocal functionals such as GGA underestimate the electronic band gap, we correct the band gaps by mixing in some percentage of exact Hartree-Fock exchange to match experimentally determined values. Here, for all three systems, we get reasonably close to the experimental values (<0.2 eV) with 10% Hartree-Fock exchange. However, no significant change is observed in the transport properties.

As mentioned before, Na_2KSb and K_2CsSb, being typical photocathode materials, are sensitive to high temperature, whereas Li_2NaSb can easily sustain 1100 K. Therefore, we focus on only room temperature applications of Na_2KSb and K_2CsSb and applications from room temperature to as high as

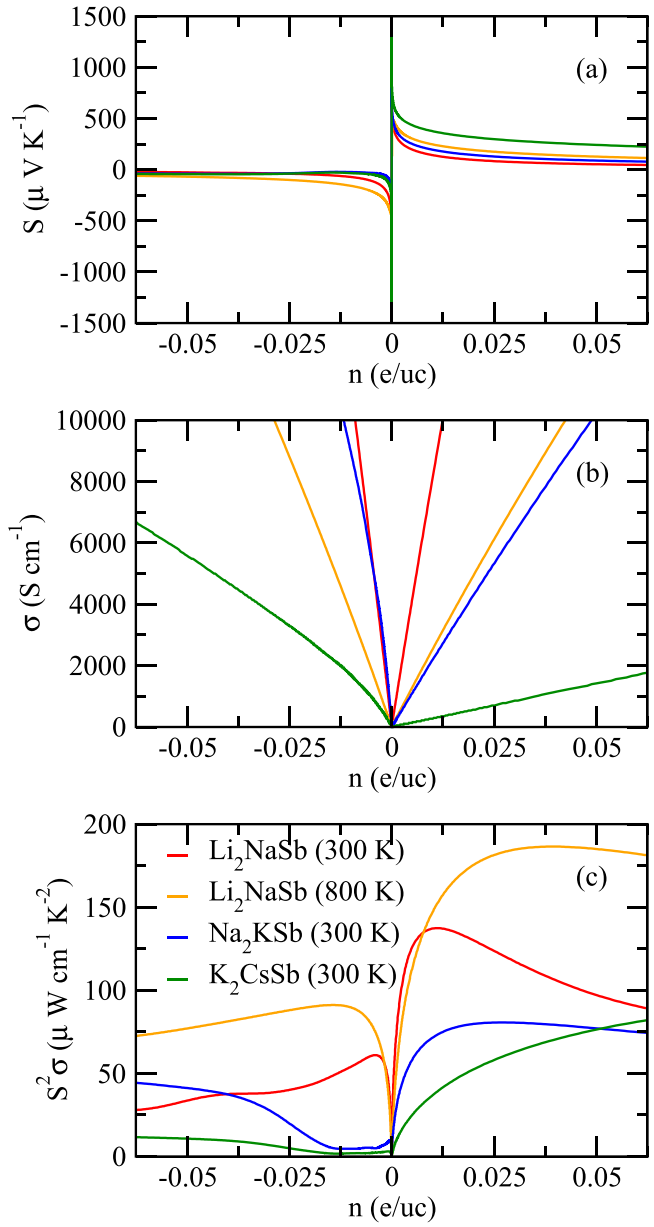

FIG. 5. (a) Seebeck coefficient S, (b) electrical conductivity σ, and (c) power factor $S^2\sigma$ for Li_2NaSb, Na_2KSb, and K_2CsSb.

1100 K for Li_2NaSb. Figure 5 shows the transport coefficients as a function of doping for all three systems at 300 K and at 800 K for Li_2NaSb. All three systems show better power factor (PF) with p-type compared to n-type doping. As these systems are soft, as indicated by their bulk modulus values (Table I), we explore only up to 5% electron or hole doping. The optimal doping corresponding to maximum PF ranges from 0.011 to 0.050 hole doping per unit cell (e uc^{-1}), which is quite reasonable since these are soft materials, as indicated by their low values of bulk modulus (Table I).

For a quantitative evaluation, it is important to determine τ_e, the electronic lifetime, which within a good approximation, can be expressed as $\frac{1}{\tau_e} = \frac{1}{\tau_{e\text{-}e}} + \frac{1}{\tau_{e\text{-ph}}}$, where $\tau_{e\text{-}e}$ and $\tau_{e\text{-ph}}$ are the lifetimes of electron-electron and electron-phonon scattering processes. It is understood that a perfect lattice yields no resistivity. One obtains resistivity if there are either (i) deviations from the perfect lattice, i.e., lattice vibrations, defects, or impurities, or (ii) electron-electron interactions. Although one would expect the e^--e^- interactions to dominate the scattering mechanisms, it is trivial to show that, owing to Pauli's principle, for materials that are not strongly correlated, the phase space of e-e scattering processes and, as a resulting, the magnitude of $\tau_{e\text{-}e}^{-1}$ are quite small in comparison to other mechanisms. Hence, for most materials, the dominant scattering mechanisms involve electron-phonon coupling.

We calculate the real and imaginary parts of the electron self-energy $\Sigma_{n\mathbf{k}} = \Sigma'_{n\mathbf{k}} + \iota\Sigma''_{n\mathbf{k}}$ within the Migdal approximation ($\omega_0/E_F \ll 1$) [42],

$$\sum_{n\mathbf{k}}(\omega, T) = \sum_{\mathbf{m}\nu}\int_{\mathrm{BZ}}\frac{d\mathbf{q}}{\Omega_{\mathrm{BZ}}}\left|g^{\nu}_{mn}(\mathbf{kq})\right|^2 \times\left[\frac{n_{\mathbf{q}\nu}(T) + f_{m\mathbf{k}+\mathbf{q}}(T)}{\omega - (\epsilon_{m\mathbf{k}+\mathbf{q}} - \epsilon_F) + \omega_{\mathbf{q}\nu} + \iota\eta} + \frac{n_{\mathbf{q}\nu}(T) + 1 - f_{m\mathbf{k}+\mathbf{q}}(T)}{\omega - (\epsilon_{m\mathbf{k}+\mathbf{q}} - \epsilon_F) - \omega_{\mathbf{q}\nu} + \iota\eta}\right],$$

as implemented in EPW. Here, Ω_{BZ} is the volume of the Brillouin zone, η is the broadening, and $f_{m\mathbf{k}}$ and $n_{q\nu}$ are the occupation factors in Fermi and Bose-Einstein statistics, respectively. Finally, $g^{\nu}_{mn}(\mathbf{kq}) = \frac{1}{\sqrt{2\omega_{\mathbf{q}\nu}}}\langle\psi_{m\mathbf{k}+q}|\partial_{q\nu}V|\psi_{n\mathbf{k}}\rangle$ is the e-ph coupling matrix element corresponding to Kohn-Sham quasiparticles represented by $\psi_{m\mathbf{k}+q}$ and $\psi_{n\mathbf{k}}$, where n is the band index and k is the wave vector in reciprocal space with $q = k' - k$. $\partial_{q\nu}V$ is the derivative of the self-consistent potential V associated with a phonon of wave vector q and branch ν with frequency $\omega_{q\nu}$. The electron lifetimes due to e-ph scattering processes are then just $\tau_{n\mathbf{k}} = \frac{\hbar}{2\Sigma''_{n\mathbf{k}}}$.

As the scattering mechanisms are temperature dependent, within the EPW framework, temperature is introduced as a parameter that affects the occupation factors. It can also become quite computationally expensive to achieve convergence for τ_e with respect to k and q grids; hence, we calculate it only at the relevant temperatures for each system. For Li_2NaSb, 8.85×10^{-14} and 3.08×10^{-14} s are the electronic relaxation times at 300 and 800 K, respectively. For Na_2KSb and K_2CsSb, we calculate τ_e only at 300 K and find values of 8.13×10^{-14} and 2.29×10^{-14} s, respectively. Utilizing these values of τ_e, the optimal doping levels and corresponding S, σ, PF, and ZT at 300 K are listed in Table III.

The Seebeck coefficient and electrical conductivity values range from 132 to 242 μV K^{-1} and 1466 to 9454 S cm^{-1}, respectively. The numbers for electrical transport are quite impressive, and coupled with low κ_L values, we obtain good ZT values. While ZT values for Li_2NaSb and Na_2KSb are still less than 1, K_2CsSb boasts a superlative value of 2.49, owing to its extremely low lattice thermal conductivity as well as it electronic thermal conductivity value, which is comparatively much lower than that of the other two alloys. As discussed before, although we are restricted to the room temperature domain for these alloys, such ZT values do merit exploration of their use as room temperature thermoelectrics.

TABLE III. Calculated optimal doping levels and the corresponding Seebeck coefficient, electrical conductivity, power factor, thermal conductivity, and figure of merit of *p*-type Li_2NaSb, Na_2KSb, and K_2CsSb at 300 K. The values in parentheses are at 800 K. Here, + and − indicate hole and electron doping, respectively. Note that the κ_L used has undoped compositions for our systems. The experimentally reported values for Fe_2VAl are included for comparison.

System	n (e uc^{-1})	S (μV K^{-1})	σ (S cm^{-1})	$S^2\sigma$ (μW cm^{-1} K^{-2})	$\kappa = \kappa_e + \kappa_L$ (W m^{-1} K^{-1})	ZT
Fe_2VAl	−0.08	120	4464	61	14	0.13
Li_2NaSb	+0.011 (0.039)	132 (144)	9454 (9282)	164 (192)	10.21 (16.24)	0.48 (0.94)
Na_2KSb	+0.028	121	6004	88	4.60	0.57
K_2CsSb	+0.050	242	1466	86	1.02	2.49

IV. SUMMARY

We have investigated the potential of Li_2NaSb, Na_2KSb, and K_2CsSb as room temperature thermoelectric materials. While it had already been predicted that the electronic properties should be favorable in the case of Li_2NaSb and K_2CsSb, we have analyzed in detail the thermal transport and predicted very low values of lattice thermal conductivity for all three alloys, especially in the case of Na_2KSb and K_2CsSb. The origin of this was found in the bonding nature and phonon transport. Especially in K_2CsSb, where the thermal conductivity is lowest, rattling modes due to soft bonding lead to high anharmonicity in the system. Looking at the phonon transport reveals that all three systems show sufficiently low υ_s and τ_{ph} values to support the determined values of κ_L. We have also provided a more detailed description of the electronic transport properties. For Li_2NaSb in particular this leads to a power factor $\gtrsim$100 μW cm^{-1} K^{-2}. Alkali and alkaline earth metal based materials with soft bonding, as also exhibited by Na_2MgSn [43] ($P6_3/mmc$), in general provide an interesting avenue for the discovery of new thermoelectric materials.

ACKNOWLEDGMENTS

Computations were performed at the Computer Centre, IIT Roorkee, India, and at IFW Dresden, Germany. We thank U. Nitzsche for technical assistance. J.v.d.B. acknowledges support from the DFG through the Würzburg-Dresden Cluster of Excellence on Complexity and Topology in Quantum Matter, ct.qmat (EXC 2147, Project No. 390858490) and through SFB 1143 (Project No. 247310070) Project No. A5.

[1] J. He, M. Amsler, Y. Xia, S. S. Naghavi, V. I. Hegde, S. Hao, S. Goedecker, V. Ozolins, and C. Wolverton, Phys. Rev. Lett. **117**, 046602 (2016).
[2] K. Berland, O. M. Løvvik, and R. Tranås, Appl. Phys. Lett. **119**, 081902 (2021).
[3] Y. Nishino, S. Deguchi, and U. Mizutani, Phys. Rev. B **74**, 115115 (2006).
[4] M. Vasundhara, V. Srinivas, and V. V. Rao, Phys. Rev. B **77**, 224415 (2008).
[5] J. Skoug, C. Zhou, Y. Pei, and D. T. Morelli, J. Electron. Mater. **38**, 1221 (2009).
[6] Y. Terazawa, M. Mikami, T. Itoh, and T. Takeuchi, J. Electron. Mater. **41**, 1348 (2012).
[7] M. Mikami, Y. Kinemuchi, K. Ozaki, Y. Terazawa, and T. Takeuchi, J. Appl. Phys. **111**, 093710 (2012).
[8] G. Xing, J. Sun, Y. Li, X. Fan, W. Zheng, and D. J. Singh, Phys. Rev. Mater. **1**, 065405 (2017).
[9] A. H. Sommer, Appl. Phys. Lett. **3**, 62 (1963).
[10] W. H. McCarroll and R. E. Simon, Rev. Sci. Instrum. **35**, 508 (1964).
[11] Z. Ding, M. Gaowei, J. Sinsheimer, J. Xie, S. Schubert, H. Padmore, E. Muller, and J. Smedley, J. Appl. Phys. **121**, 055305 (2017).
[12] W.-M. Hurng, Mater. Res. Bull. **26**, 439 (1991).
[13] G. Kresse and J. Hafner, Phys. Rev. B **47**, 558 (1993).
[14] G. Kresse and J. Hafner, Phys. Rev. B **49**, 14251 (1994).
[15] G. Kresse and J. Furthmüller, Comput. Mater. Sci. **6**, 15 (1996).
[16] G. Kresse and J. Furthmüller, Phys. Rev. B **54**, 11169 (1996).
[17] J. P. Perdew, K. Burke, and M. Ernzerhof, Phys. Rev. Lett. **77**, 3865 (1996).
[18] J. P. Perdew, K. Burke, and M. Ernzerhof, Phys. Rev. Lett. **78**, 1396(E) (1997).
[19] P. E. Blöchl, Phys. Rev. B **50**, 17953 (1994).
[20] G. Kresse and D. Joubert, Phys. Rev. B **59**, 1758 (1999).
[21] A. Togo and I. Tanaka, Scr. Mater. **108**, 1 (2015).
[22] A. Togo, L. Chaput, and I. Tanaka, Phys. Rev. B **91**, 094306 (2015).
[23] L. Chaput, Phys. Rev. Lett. **110**, 265506 (2013).
[24] G. K. H. Madsen, J. Carrete, and M. J. Verstraete, Comput. Phys. Commun. **231**, 140 (2018).
[25] S. Poncé, E. R. Margine, C. Verdi, and F. Giustino, Comput. Phys. Commun. **209**, 116 (2016).
[26] P. Giannozzi *et al.*, J. Phys.: Condens. Matter **21**, 395502 (2009).
[27] P. Giannozzi *et al.*, J. Phys.: Condens. Matter **29**, 465901 (2017).
[28] O. Jepsen and O. K. Andersen, STUTTGART TB-LMTO-ASQA program, version 4.7, Max-Planck-Institut für Festkörperforschung, Stuttgart, Germany, 2000.
[29] C. Ghosh and B. P. Varma, J. Appl. Phys. **49**, 4549 (1978).
[30] D. G. Fisher, A. F. McDonie, and A. H. Sommer, J. Appl. Phys. **45**, 487 (1974).

[31] M. Zeeshan, T. Nautiyal, J. van den Brink, and H. C. Kandpal, Phys. Rev. Mater. **2**, 065407 (2018).
[32] L.-D. Zhao, S.-H. Lo, Y. Zhang, H. Sun, G. Tan, C. Uher, C. Wolverton, V. P. Dravid, and M. G. Kanatzidis, Nature (London) **508**, 373 (2014).
[33] D. G. Cahill, S. K. Watson, and R. O. Pohl, Phys. Rev. B **46**, 6131 (1992).
[34] M. T. Agne, R. Hanus, and G. J. Snyder, Energy Environ. Sci. **11**, 609 (2018).
[35] L.-D. Zhao, J. He, D. Berardan, Y. Lin, J.-F. Li, C.-W. Nan, and N. Dragoe, Energy Environ. Sci. **7**, 2900 (2014).
[36] H. C. Kandpal, C. Felser, and R. Seshadri, J. Phys. D **39**, 776 (2006).
[37] B. C. Sales, B. C. Chakoumakos, and D. Mandrus, J. Solid State Chem. **146**, 528 (1999).
[38] M. K. Jana, K. Pal, A. Warankar, P. Mandal, U. V. Waghmare, and K. Biswas, J. Am. Chem. Soc. **139**, 4350 (2017).
[39] D. T. Morelli, V. Jovovic, and J. P. Heremans, Phys. Rev. Lett. **101**, 035901 (2008).
[40] M. Christensen, A. B. Abrahamsen, N. B. Christensen, F. Juranyi, N. H. Andersen, K. Lefmann, J. Andreasson, C. R. H. Bahl, and B. B. Iversen, Nat. Mater. **7**, 811 (2008).
[41] See Supplemental Material at http://link.aps.org/supplemental/10.1103/PhysRevMaterials.6.125401 for the electronic band structure, density of states, and phonon lifetime for Li_2NaSb, Na_2KSb, and K_2CsSb.
[42] A. B. Migdal, J. Exptl. Theoret. Phys. (U.S.S.R.) **34**, 1438 (1958).
[43] C. Wang, Y. B. Chen, S.-H. Yao, and J. Zhou, Phys. Rev. B **99**, 024310 (2019).